Optimizing a High Lateral Misalignment Tolerance of the Short-range Inductive Coupling Wireless Power Transfer System by Using Basic Capacitive Compensation Topologies

Deeb ALASHGAR[1], Koji FUJIWARA[2], and Yasuhito TAKAHASHI[3]

[1,2,3]*Department of Electrical & Electronic Engineering, Doshisha University*

Abstract - An Inductive Wireless Power Transfer (IWPT) system is enhanced to have high lateral misalignment tolerance. Analytical and experimental comparison among the four basic capacitive compensation (CC) topologies is made to get the appreciated and optimized high lateral misalignment tolerance of the IWPT system. These four basic topologies are the Series-Series (SS-CC), the Parallel-Series (PS-CC), the Series-Parallel (SP-CC), and the Parallel-Parallel (PP-CC) topologies. The SS-CC topology is the most appropriate method for optimizing a high lateral misalignment tolerance in the IWPT system. Its advantages include the independence of its resonance frequency of the misalignment in addition to having high voltage and current gains in addition to having a zero phase shift angle at any misalignment, which is better for low switching losses.

Keywords: *Inductive Wireless Power Transfer (IWPT), Series-Series Capacitive Compensation (SS-CC), Parallel-Series Capacitive Compensation (PS-CC), Series-Parallel Capacitive Compensation (SP-CC), Parallel-Parallel Capacitive Compensation (PP-CC), Lateral misalignment tolerance.*

1. INTRODUCTION

Researchers shed light on power transfer without wires as it has multi economic and environmental benefits; for instance, the safety and the ease of maintenance. The method of transferring power wirelessly depends on different factors such as the safety and the distance between the power source and the system's load. Although the methods of transferring power wirelessly through microwaves [1], laser waves [2] [3] [4], or the electric field [5] is secure. the magnetic field is considered to be the most secure at specific frequencies [6]. In the Inductive Wireless Power Transfer (IWPT) system, the efficiency is optimized by both the shape [7] [8] and the capacitive compensations. The capacitive compensation parts can be connected in series or parallel in both sides of the IWPT system that leads to four basic topologies of capacitive compensation which are the SS-CC [9] [10] [11], PS-CC, SP-CC, and PP-CC topologies.

In this paper, the IWPT system is investigated according to its positive impacts that match the requirements of the new electric systems[12]. The IWPT system transfers power from the primary coil to the secondary coil through a magnetic field, with different types of planar geometry coils such as circular or rectangular. Yet, although circular geometry shows better coupling between the primary and secondary coils of the IWPT transformer [13], this research focuses on rectangular geometry because of high tolerance to misalignment between the primary and secondary coils of the IWPT transformer which holds the optimum capacitive compensated IWPT system.

2. THEORETICAL ANALYSIS

The short-range IWPT system is used to transfer power from the primary coil to the secondary coil without a physical connection. As shown in Figure 1, the primary side of the induction circuit consists of an internal resistance r_1 and a self-inductance L_1 and the secondary side circuit also composes of an internal resistance r_2 and a self-inductance L_2. Both sides are coupled by a mutual inductance M. When an alternating voltage V_{in} is applied to the primary coil, a current I_2 flows in the secondary coil which is connected to resistive load R_L.

$$V_{in} = E_m \sin(\omega t + \theta) \text{ [V]} \quad (1)$$

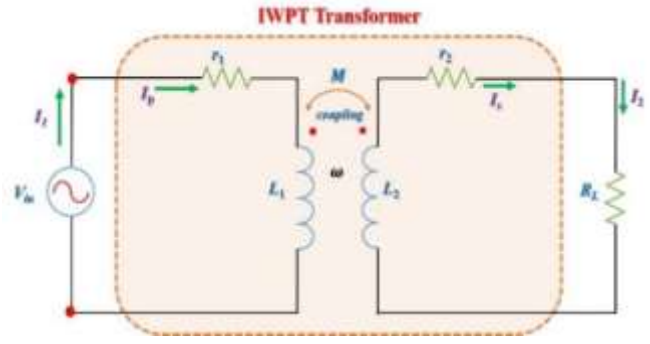

Figure 1. The short-range IWPT system.

The IWPT systems are improved by enhancing the coupling between transmitting and receiving coils. Figure 2 shows that the coupling enhancement in the IWPT systems can be achieved by high lateral

misalignment tolerance geometry design as well as through the phenomenon of resonance. As mentioned earlier, coils with square and rectangular geometries are better for misalignment tolerance. Therefore, the square shape was chosen as a suitable design for this research since the research focuses on developing the misalignment tolerance of the IWPT system.

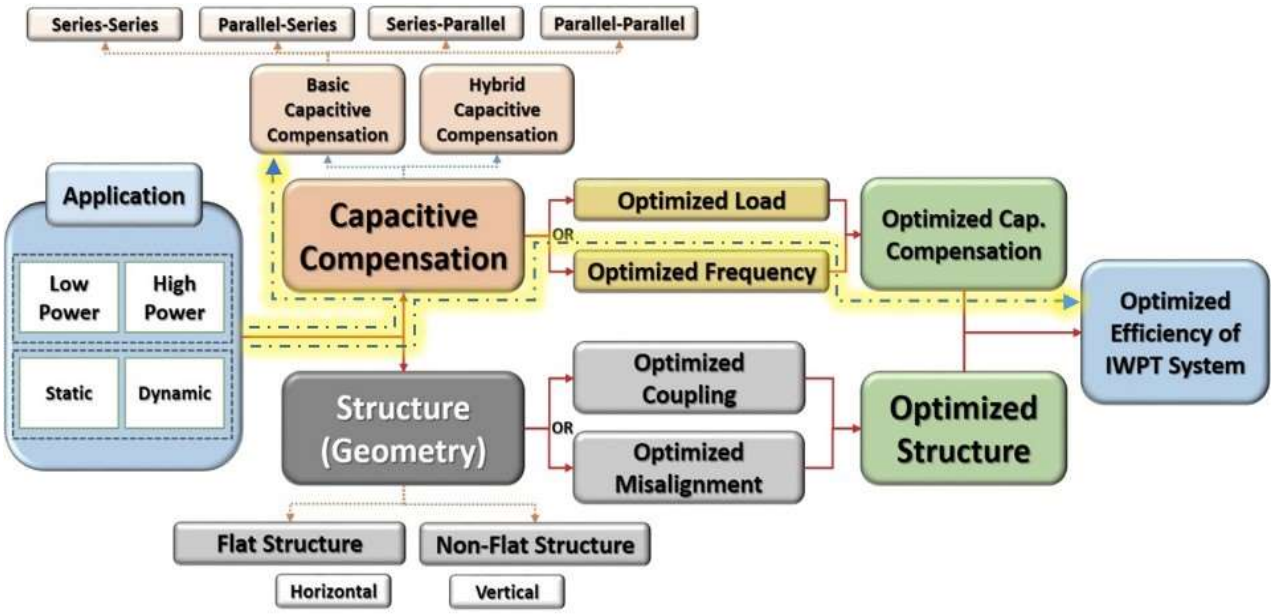

Figure 2. Block diagram for optimizing the IWPT system.

The resonance phenomenon can be implemented in the IWPT systems by connecting the capacitors in parallel or series with the IWPT's coils to suppress the drop in efficiency that occurs due to power losses. These connections result in four basic topologies for capacitive compensation. Each of which has its advantages and disadvantages. These four capacitive compensation topologies are used to imply the resonance phenomena. Figure 3 shows the four basic topologies. They are discussed because of their advantages in terms of small size and low cost.

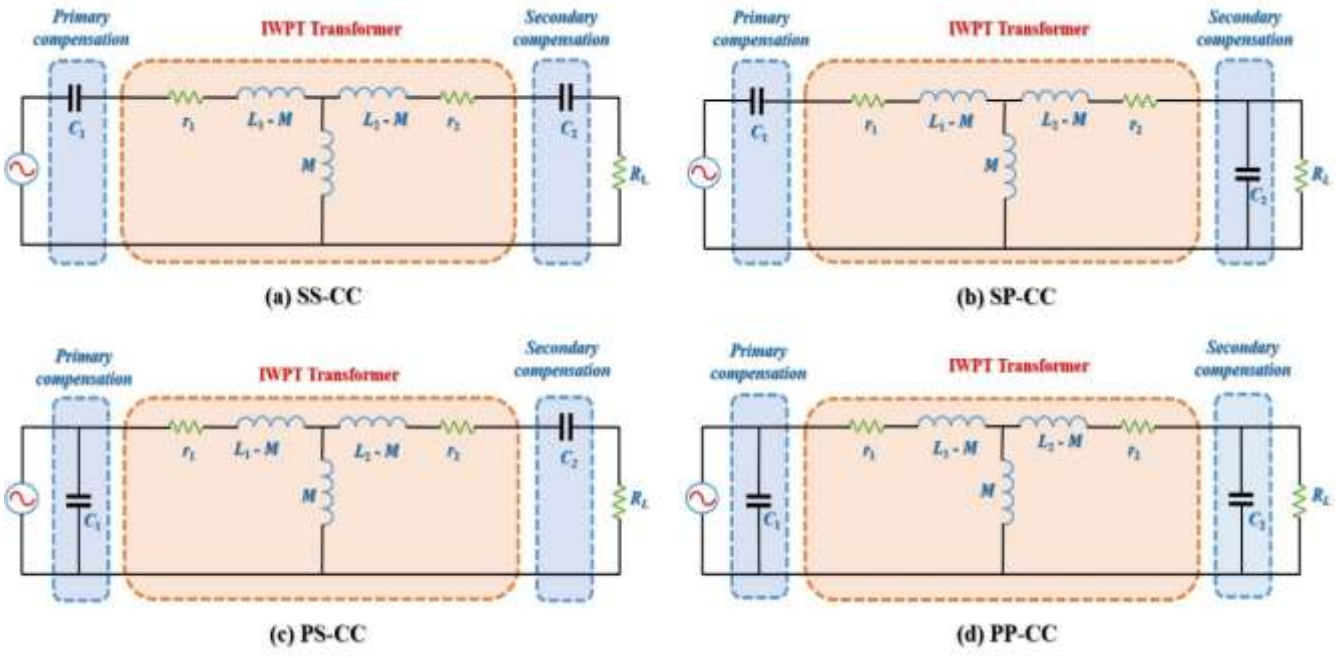

Figure 3. The capacitive compensation topologies of the IWPT systems.

While a knowledge of the characteristics of the resonant circuit and its resonant frequency properties is essential, there are many theoretical analysis ways for the multi-resonant circuits. Therefore, the two-port network analysis has been expressed as a simple analysis method for analyzing the complex resonant circuits. The analysis using the two-port network circuit started in the 1920s [14]. The fundamental parameters of the total network are as flows:

$$\begin{bmatrix} V_1 \\ I_1 \end{bmatrix} = \begin{bmatrix} F_{11} & F_{12} \\ F_{21} & F_{22} \end{bmatrix} \begin{bmatrix} V_2 \\ I_2 \end{bmatrix}. \quad (1)$$

The total system's fundamental parameter matrix [F_{all}] is defined as follows:

$$[F_{all}] = \begin{bmatrix} F_{11} & F_{12} \\ F_{21} & F_{22} \end{bmatrix}. \quad (2)$$

In the overall resonance circuits, the F parameters of each resonance circuit with its capacitive compensation are divided into two F parameters, F_p and F_s, which are called primary fundamental parameters and secondary fundamental parameters respectively. The overall fundamental parameters [F_{all}] are presented as a cascaded of both of the primary and secondary fundamental parameters as follows:

$$[F_{all}] = [F_p] * [F_s] = \begin{bmatrix} F_{11} & F_{12} \\ F_{21} & F_{22} \end{bmatrix}. \quad (3)$$

Each capacitive compensation side is connected in series or parallel with the IWPT transformer to obtain the phenomenon of resonance on both sides of the system. In terms of the capacitance for the primary capacitive compensation (C_1), equation (4) shows fundamental matrix parameters of primary series capacitive compensation cascaded with the mutual inductance, while equation (5) shows fundamental matrix parameters of primary series capacitive compensation with the mutual inductance, as follows:

$$F_{P_S} = \begin{bmatrix} r_1 + j\omega L_1 + \frac{1}{j\omega C_1} & r_1 + j\omega\left(L_1 - M - \frac{1}{C_1}\right) \\ \frac{1}{j\omega M} & 1 \end{bmatrix}, \quad (4)$$

$$F_{P_P} = \begin{bmatrix} \frac{r_1 + j\omega L_1}{j\omega M} & r_1 + j\omega(L_1 - M) \\ j\omega C_1 + \frac{1 + j\omega C_1(r_1 + j\omega(L_1 - M))}{j\omega M} & 1 + j\omega C_1(r_1 + j\omega(L_1 - M)) \end{bmatrix}. \quad (5)$$

On the other hand, in terms of the capacitance for the secondary capacitive compensation(C_2), equation (6) shows fundamental matrix parameters of secondary series capacitive compensation, while equation (7) shows fundamental matrix parameters of secondary parallel capacitive compensation as follows:

$$F_{S_S} = \begin{bmatrix} 1 & r_2 + R_L + j\omega(L_2 - M) + \frac{1}{j\omega C_2} \\ 0 & 1 \end{bmatrix}, \quad (6)$$

$$F_{S_P} = \begin{bmatrix} 1 + j\omega C_2\left(r_2 + j\omega(L_2 - M)\right) + \left(\frac{r_2 + j\omega(L_2 - M)}{R_L}\right) & r_2 + j\omega(L_2 - M) \\ j\omega C_2 + \frac{1}{R_L} & 1 \end{bmatrix}. \quad (7)$$

In terms of Figure 3 and equation (1), the impedance (Z_{in}) and phase shift (θ) from the input side are expressed by equation (8) and equation (9), respectively as follows:

$$Z_{in} = \frac{V_1}{I_1} = \frac{V_1}{V_2} * \frac{V_2}{I_1} = \left|\frac{F_{11}}{F_{21}}\right|, \quad (8)$$

$$\theta = \tan^{-1}\left\{\frac{\mathrm{Im}(Z_{in})}{\mathrm{Re}(Z_{in})}\right\}. \quad (9)$$

The output current can be expressed by the relationship between the voltage of the output and its impedance as shown in equation (10):

$$I_2 = \frac{V_2}{R_L}. \quad (10)$$

Both of the voltage gain A_V and current gain A_I can also be expressed by the ratio of V_2 and V_1, and the ratio of I_2 and I_1, respectively, which can be calculated by using both of equation (2) and equation (10) as follows:

$$A_V = \frac{V_2}{V_1} = \frac{R_L}{(R_L F_{11}) + F_{12}}, \quad (11)$$

$$A_I = \frac{I_2}{I_1} = \frac{1}{(R_L F_{21}) + F_{22}}. \quad (12)$$

The efficiency (η) of the IWPT system is the product of both the voltage gain A_V and current gain A_I as follows:

$$\eta = A_V * A_I * 100. \quad (13)$$

3. RESULTS and DISCUSSION

The multifunction generator (NF, WF-1974) is utilized to generate the 100 kHz signals. It is connected to the high-speed bipolar amplifier (NF, HSA 4014), which provides power to the IWPT system with 50 W. Furthermore, Litz wires are used to make the windings as shown in Figure 4. The configuration of the transmitter and receiver coils is illustrated in Figure 5. Their specifications are shown in Table 1.

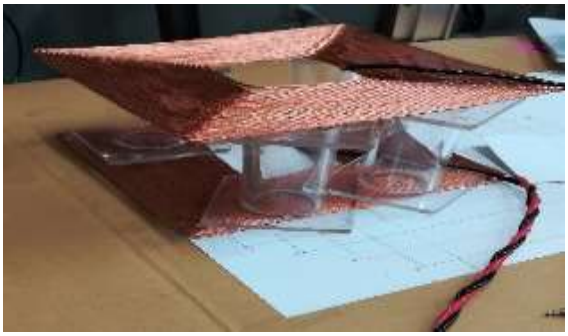

Figure 4. The experimental coils of the IWPT system.

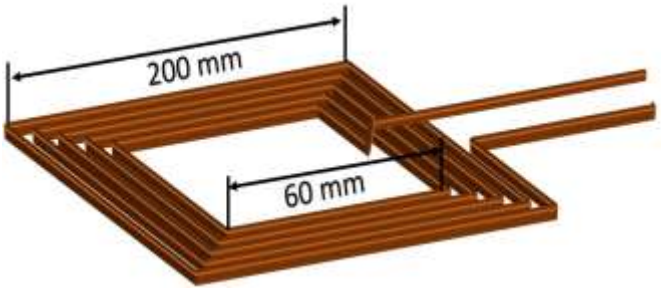

Figure 5. The coil's configurations.

Table 1. The configuration of the transmitter and receiver coils of the IWPT system.

Compressions	Primary coil	Secondary coil
Inner diameter [mm]	60	60
Outer diameter [mm]	200	200
Number of winding Turns [turns]	32	32
Self-inductance [μH]	0.1585	0.1633
Impedance [Ω]	0.36	0.41
Resonance freq. [kHz]	100	
Input voltage (V_1) [V]	20	
Load (R_L) [Ω]	100	

As a numerical discussion of the misalignment issue of the IWPT system, the capacitance value of the capacitive compensation should be taken into consideration. When the secondary capacitive compensation is set for all the basic topologies as shown in equation (14):

$$C_2 = \frac{1}{{\omega_o}^2 L_2}, \qquad \omega_{o2} = \frac{1}{\sqrt{C_2 L_2}}. \tag{14}$$

Considering that the inductance ratio L_n is the ratio of primary inductance to secondary inductance, the primary capacitive compensation for all topologies is expressed in Table 2 which figures out that the SS-CC topology at the resonance on the primary side does not depend on the coupling between the coils. The others get affected by it directly. Generally, any misalignment will affect strongly all the capacitive compensation topologies except the SS-CC topology. While the resonance frequencies of the rest of the topologies are greatly affected by the coupling factor (k), conceding that any misalignment effect on the capacitance values will significantly affect the resonance frequency too.

Table 2. The comparison of the four basic topologies in terms of capacitive compensation of the primary side and its resonance frequency.

Topo-logy	Primary capacitance (C_1)	Primary resonance frequency
SS	$\frac{C_2}{L_n}$	$\frac{1}{\sqrt{\frac{C_2 L_1}{L_n}}} = \frac{1}{\sqrt{C_2 L_2}}$
PS	$\frac{{R_L}^2 {C_2}^2}{L_n({R_L}^2 C_2 + k^4 L_2)}$	$\frac{1}{\sqrt{\frac{{R_L}^2 {C_2}^2 L_2}{({R_L}^2 C_2 + k^4 L_2)}}}$
SP	$\frac{C_2}{L_n(1-k^2)}$	$\frac{1}{\sqrt{\frac{C_2 L_2}{(1-k^2)}}}$
PP	$\frac{(1-K^2)L_2 C_2}{L_n(L_2(1-K^2)^2 + K^4 {R_L}^2 C_2)}$	$\frac{1}{\sqrt{\frac{(1-K^2){L_2}^2 C_2}{(L_2(1-K^2)^2 + K^4 {R_L}^2 C_2)}}}$

After analyzing the circuits shown in Figure 3 by Frequency Response Analysis (FRA) method, Figure 6 presents the behavior of the four topologies in terms of the frequency. It shows that the primary parallel capacitive compensation gives more efficiency than the primary series capacitive compensation. On the contrary, the primary series capacitive compensation delivers more power with a higher voltage gain than the primary parallel capacitive compensation.

Figure 7 presents the behavior of the four topologies as a function of misalignment. It shows that the primary parallel capacitive compensation gives more efficiency than the primary series capacitive compensation. On the contrary, the primary series capacitive compensation delivers more power with a higher voltage gain than the primary parallel capacitive compensation, but little misalignment significantly affects the delivered power of the IWPT system with primary parallel capacitive compensation more than the IWPT system with primary series capacitive compensation. In the case of the input impedance, the misalignment affects all the topologies, but the secondary series capacitive compensation gives more stability. At the same time, it shows that the SP-CC provides stable current gain, where the others need current controllers. The advantage of the SS-CC is figured out in phase shift variation as a function of misalignment; it is not affected by the misalignment, while the rest of the topologies are affected. Figure 8 shows the experimental results of the SS-CC topology as a function of misalignment. The experiments are carried

out to investigate the analytical result. It is noticed that the voltage gain is inversely proportional to the misalignment, while the current gain is proportional to the misalignment. In the case of the phase shift and input impedance, the misalignment has little effect. It influence can be neglected, and the system can be considered an excellent power transfer system.

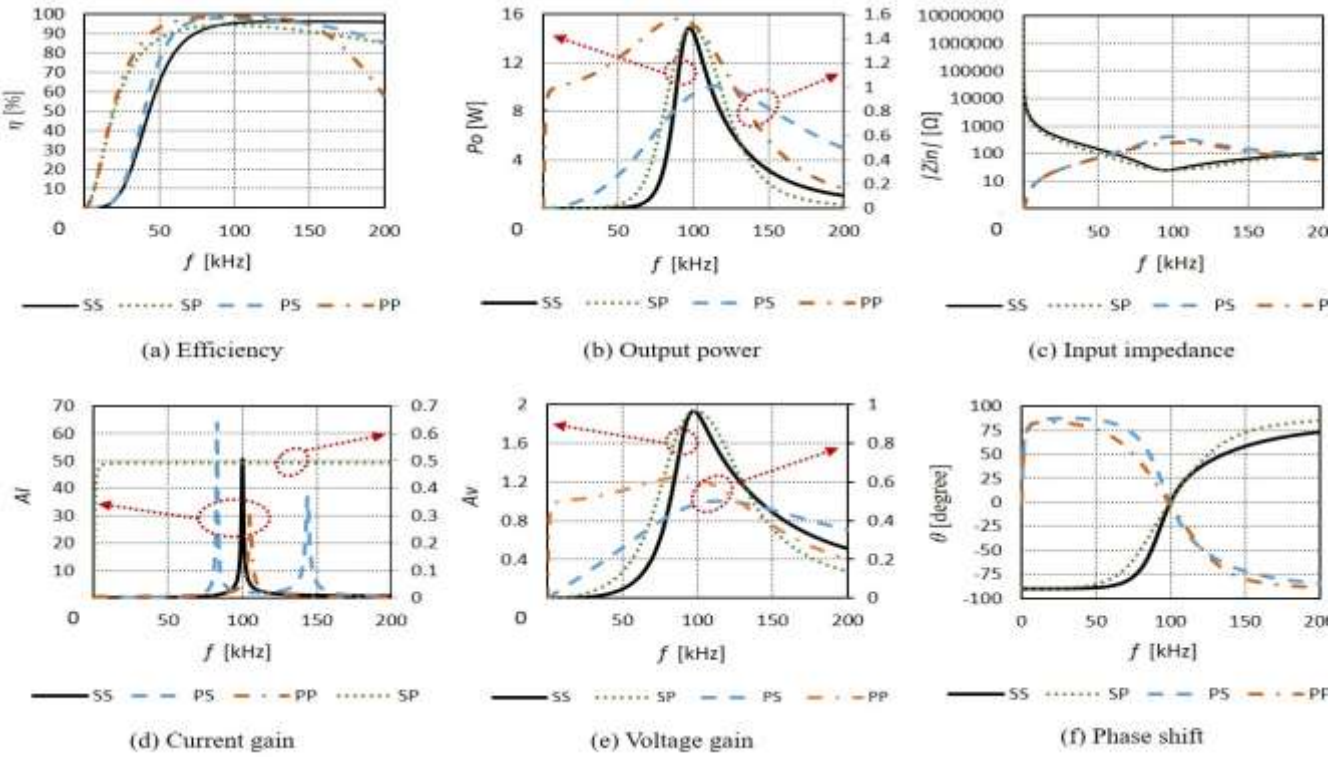

Figure 6 The comparison among all topologies in terms of frequency.

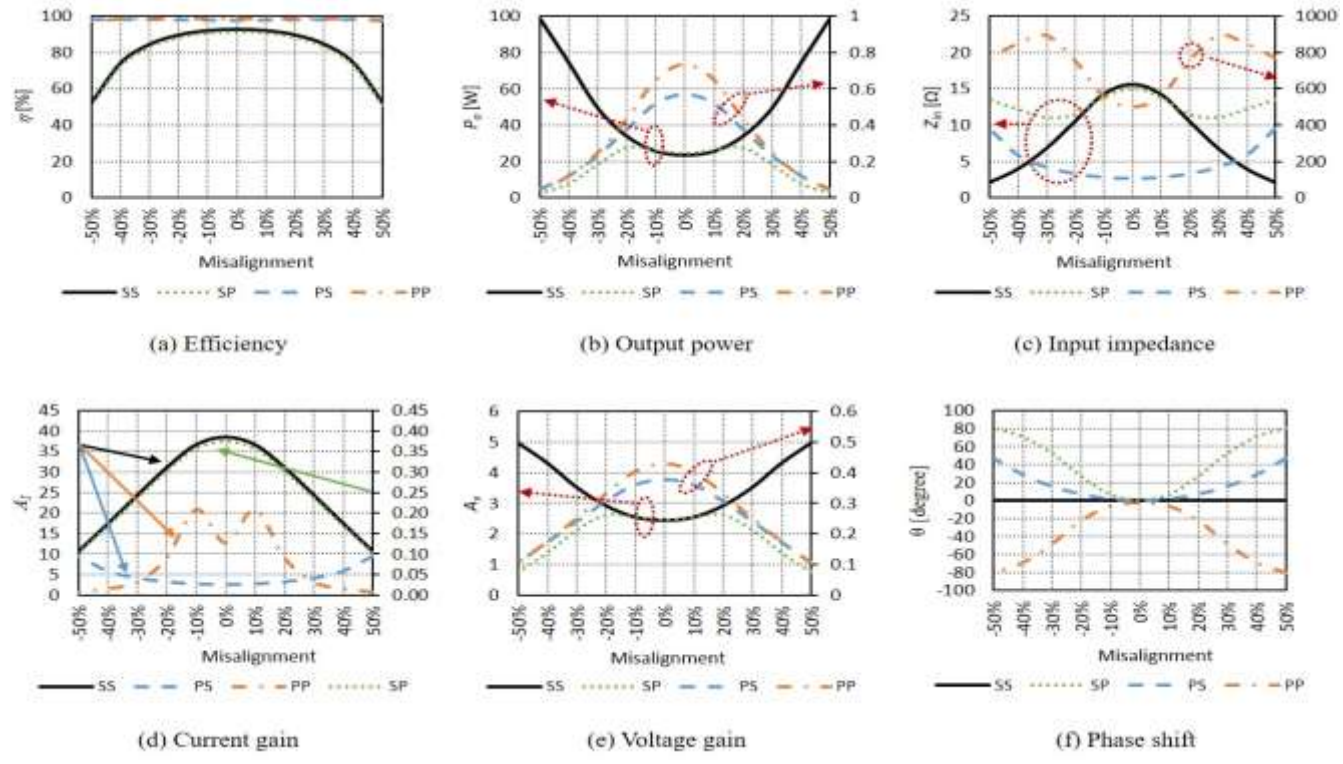

Figure 7. The comparison among all topologies in terms of horizontal one-axis misalignment.

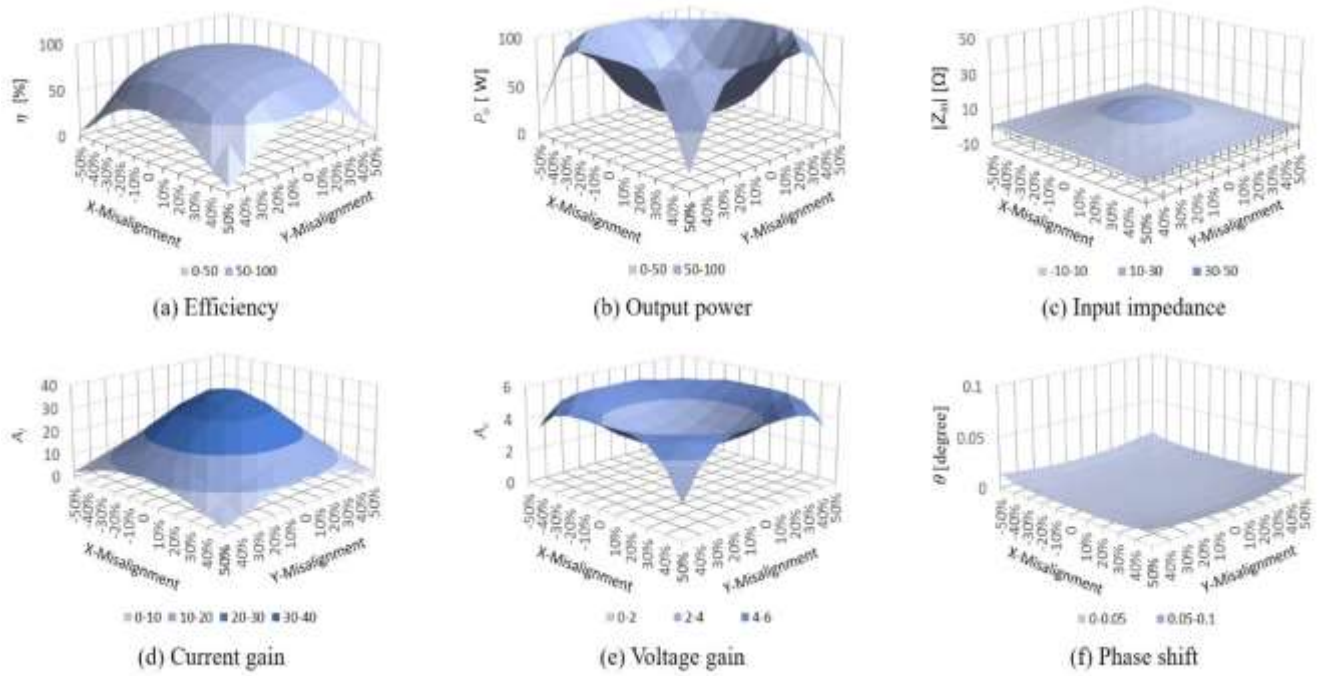

Figure 8. The SS-CC topology as a function of misalignment.

Figure 9, Figure 10, and Figure 11 illustrate the experimental results of the PS-CC, SP-CC, and PP-CC, respectively. The behavior of the system is affected so much in these three capacitive compensations. The power delivered by using the SP-CC topology is higher than the PS-CC, and the PP-CC topologies. On the other hand, the effect of misalignment on the phase shift angle is significant in all of them. It is affected by both the SP-CC and SP-CC topologies so that the phase shift angle becomes more positive, which means that the system becomes more inductive. In contrast, the phase shift angle becomes a more negative and more capacitive system in the case of the PP-CC. It is also shown that current gain is not stable in the case of the PP-CC topology, but it is more stable in terms of PS-CC topology.

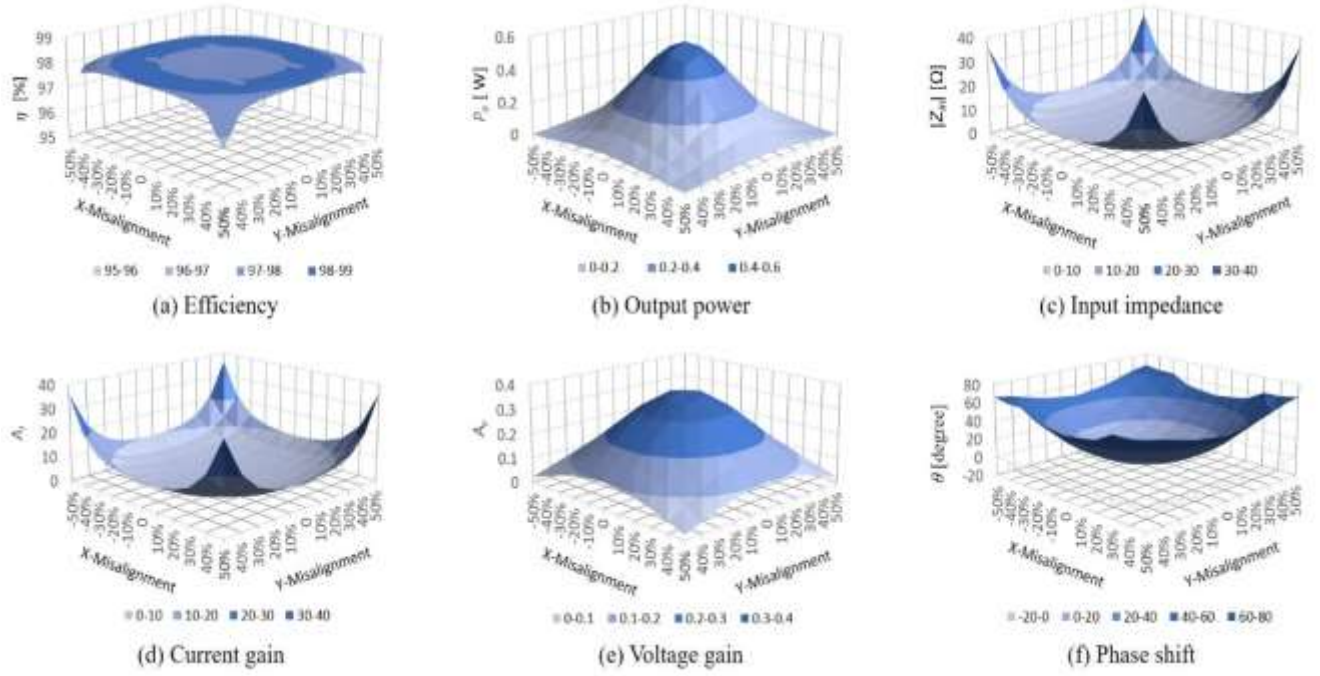

Figure 9. The PS-CC topology as a function of misalignment.

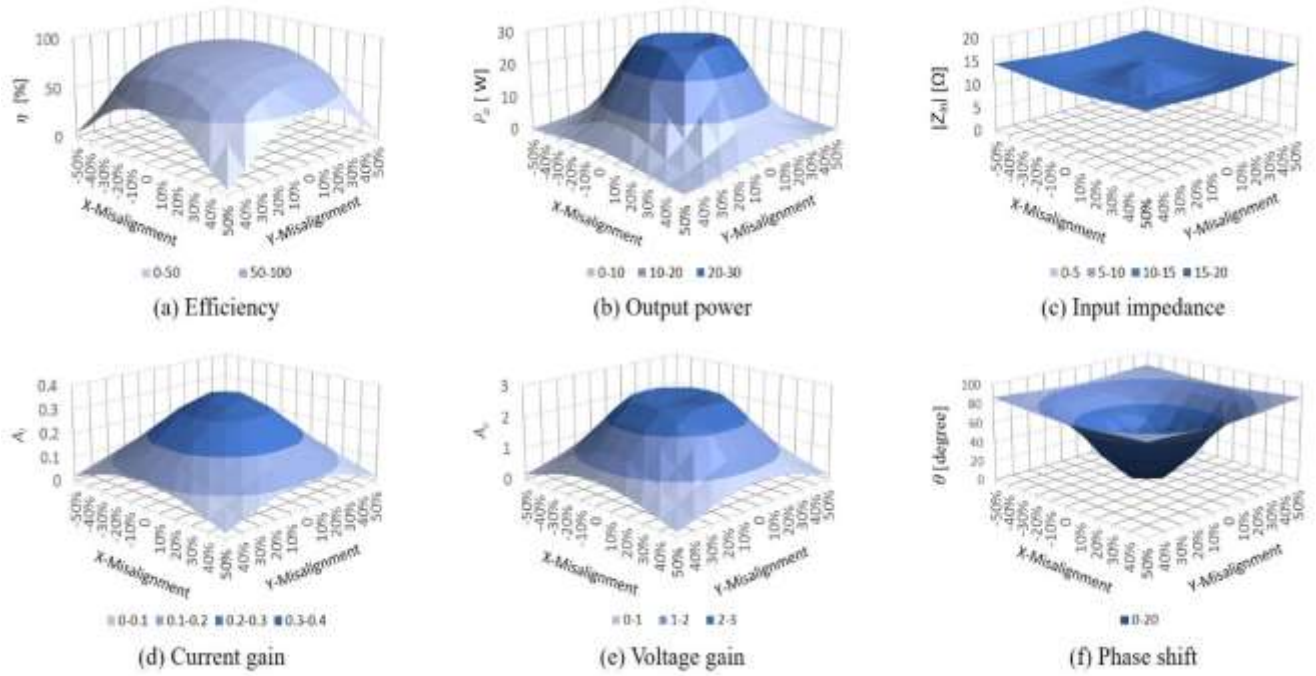

Figure 10. The SP-CC topology as a function of misalignment.

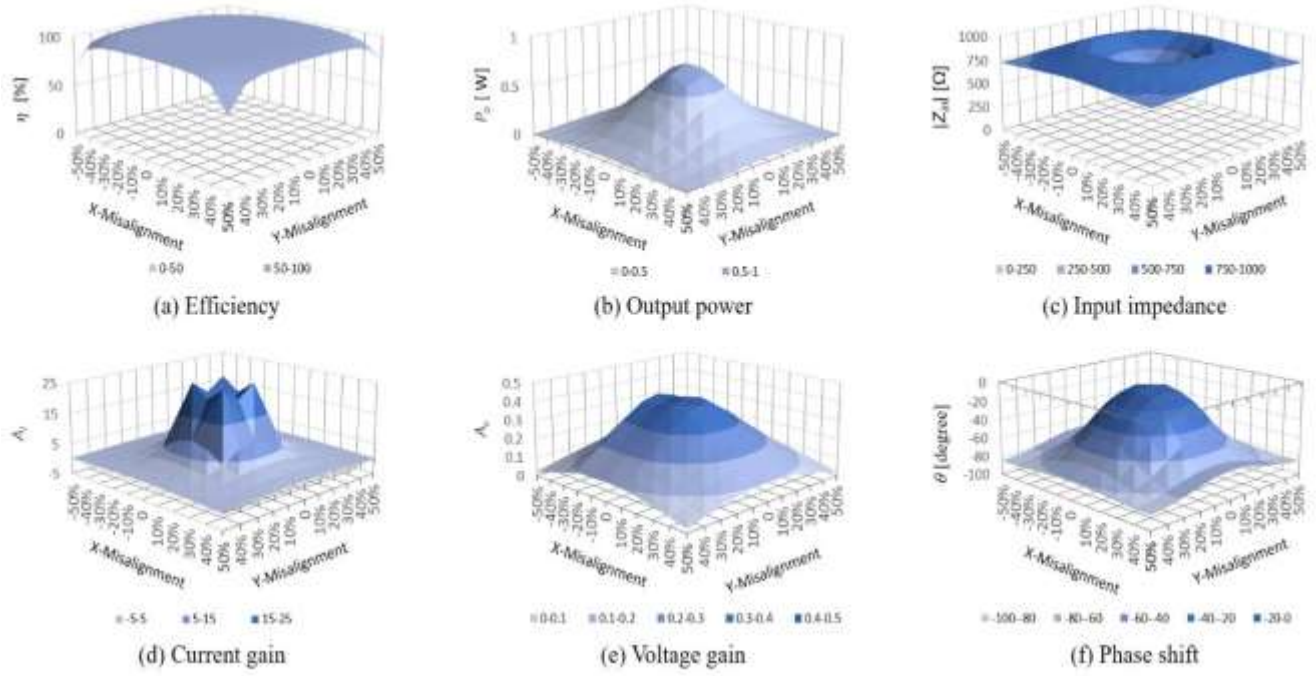

Figure 11. The PP-CC topology as a function of misalignment.

4. CONCLUSIONS

The primary series of capacitive compensation provides higher delivered power than the secondary series of capacitive compensation, while the latter gives higher tolerance to misalignment in the case of efficiency. The current is inversely proportional to the misalignment in all of the SS-CC, SP-CC and PP-CC, while it is directly proportional to the misalignment in the PS-CC. The voltage gain is inversely proportional to the misalignment in all of the SP-CC, SP-CC, and PP-CC, while it is directly proportional to the misalignment in the SS-CC until thirty percent, then starts to be decreased. Knowing that the current gain is seven times higher in the primary series of capacitive compensation than the

secondary series of capacitive compensation; in the case of the SP-CC, SP-CC and PP-CC, the effect of misalignment on the phase shift angle will be significant, as it affects both the SP-CC and SP-CC so that the phase shift angle becomes more positive, which means that the current lags the voltage, which leads to more switch losses and the need to increase the capacitive compensation, while the phase shift angle becomes more negative and needs to reduce capacitive compensation in the case of the PP-CC.

Nevertheless, it is clearly noticeable that the effect of the misalignment on the phase shift angle in the case of the SS-CC is minimal and can be neglected, which means it is the most appropriate method which provides a high lateral misalignment tolerance in the IWPT system. This paper demonstrates originality by experiments and numerical analysis proving that the SS-CC is better than other topologies in terms of power losses reduction caused by misalignment issues. This topology shows that the phase shift is not affected by misalignment and equals to zero. This means that the input current and input voltage are in phase. The analytical and experimental results are matched and show that the appreciated topology to optimize the misalignment tolerance is the SS-CC topology.

REFERENCES

[1] K. Lee, J. Kim, and C. Cha, "Microwave-based Wireless Power Transfer Using Beam Scanning for Wireless Sensors," *IEEE EUROCON 2019 -18th International Conference on Smart Technologies*, Novi Sad, Serbia, Serbia, p. 51, July 2019.

[2] A. Hertzberg, W. H. Christiansen, E. W. Johnston, and H. G. Alstrom, "Photon Generators and Engines for Laser Power Transmission," *AIAA Journal*, vol. 10, no. 4, pp. 394-400, May 2012.

[3] D. E. Raible, "High Intensity Laser Power Beaming for Wireless Power Transmission," engaged scholarship SCU, Cleveland, May 2008.

[4] K. J. Duncan, "Laser Based Power Transmission: Component Selection and Laser Hazard Analysis," *2016 IEEE PELS Workshop on Emerging Technologies: Wireless Power Transfer (WoW)*, Knoxville, TN, USA, pp. 100-103, Oct. 2016.

[5] L. J. Zou and A. P. Hu, "A Contactless Single-wire CPT (Capacitive Power Transfer) Power Supply for Driving a Variable Message Sign," *2018 IEEE PELS Workshop on Emerging Technologies: Wireless Power Transfer (Wow)*, Montreal, QC, Canada, pp. 870-875 August 2018.

[6] D. Alashgar, K. Fujiwara, and N. Nagaoka, "Fundamental Investigation of Short-range Inductive Coupling Wireless Power Transmission by Using Series-Series Capacitive Compensation Topology," *Journal of Asian Electric Vehicles*, vol. 17, no. 1, pp. 1811-1822, June 2019.

[7] J. Feng, Q. Li, and F. C.Lee, "Omnidirectional Wireless Power Transfer for Portable Devices," *2017 IEEE Applied Power Electronics Conference and Exposition (APEC)*, Tampa, FL, USA, pp. 1675-1681, March 2017.

[8] Z. Liu, Z. Chen, and J. Li, "A Magnetic Tank System for Wireless Power Transfer," *IEEE Microwave and Wireless Components Letters*, vol. 27, no. 5, pp. 443-445, April 2017.

[9] J. P.-W. Chow, and H. S.-H. Chung, "Use of Transmitter-side Electrical Information to Estimate Mutual Inductance and Regulate Receiver-side Power in Wireless Inductive Link," *IEEE Transactions on Power Electronics*, vol. 31, no. 9, pp. 6079-6091, Sept. 2016.

[10] S. Kuzey, S. Balci, and N. Altin, "Design and Analysis of a Wireless Power Transfer System with Alignment Errors for Electrical Vehicle Applications," *International Journal of Hydrogen Energy*, vol. 42, no. 28, pp. 17928-17939, July 2017.

[11] T. Campi, S. Cruciani, V. D. Santis, F. Maradei, and M. Feliziani, "Numerical Analysis Applying the AMSL Method to Predict the Magnetic Field in an EV with a WPT System," *2018 IEEE Wireless Power Transfer Conference (WPTC)*, Montreal, Canada, p. 77, June 2018.

[12] M. A. Hassan and A. Elzawawi, "Wireless Power Transfer through Inductive Coupling," *Institute for Natural Sciences and Engineering INASE*, pp. 115-118, July 2015.

[13] J. D. Boeij, E. Lomonova, and A. Vandenput, "Contactless Energy Transfer to a Moving Load Part I: Topology Synthesis and FEM simulation," *2006 IEEE International Symposium on Industrial Electronics*, Montreal, Que., Canada, pp. 739-744, July 2006.

[14] G. Saggio, *Principles of Analog Electronics*, New York: CRC Press, p. 163, 2014.

AUTHORS

Deeb E. ALASHGAR received his B.S. (2013) in electrical engineering from the Islamic University of Gaza IUG, Gaza, Palestine, and the M.S. (2017) in electrical & electronic engineering from Doshisha University, Kyoto, Japan. He is currently working on his advanced doctoral degree in Global Resource Management GRM and his Ph.D. in electrical & electronic engineering at

Doshisha University, Kyoto, Japan. His research interests include Wireless Power Transfer Systems, Electromagnetics and Power Electronics.

Koji Fujiwara was born in Hiroshima Prefecture, Japan, on 26 January in 1960. He received the B.S. and M.S. degrees in electrical engineering from Okayama University, and the D.E. degree from Waseda University, Japan, in 1982, 1984 and 1993, respectively. From 1985 to 1986, he was with Mitsui Engineering and Shipbuilding Co., Ltd. From 1986 to 2006, he was with Okayama University. Since 2006, he has been a Professor at the Department of Electrical Engineering, Doshisha University. His major fields of interest are the development of the 3-D finite element method for nonlinear magnetic field analysis including eddy currents and its application to electrical machines, and the development of standard methods of measurement of magnetic properties of magnetic materials.

Yasuhito Takahashi received B.E., M.E. and a Ph.D. degree in 2003, 2005, and 2008, respectively, at Waseda University, Tokyo, Japan. He became an assistant professor at Kyoto University and Doshisha University in 2008 and 2010, respectively. Since 2015, he has been an associate professor at Doshisha University. His current research interests are in the fast and large-scale computation of electromagnetic field, modeling of magnetic properties of magnetic materials and photovoltaic power generation system.